Full-wave simulation of ion cyclotron range of frequency heating in a mirror device

John Wright[1*], *Taosif* Ahsan[1], *Paul T.* Bonoli[1], *Yuri* Petrov[2], *Robert W.* Harvey[2], and *Sam* Frank[3]

[1]Massachusetts Institute of Technology, Cambridge, MA, USA
[2]CompX Co., Del Mar, CA, USA
[3]Realta Fusion, Madison, WI, USA

Abstract. We are adapting the all-orders spectral algorithm (AORSA) [Jaeger Phys. Plasmas **8** (2001)] from tokamak geometry to axisymmetric magnetic mirror geometry. We will use the modified AORSA to study ion cyclotron range of frequency (ICRF) heating in the Wisconsin HTS Axisymmetric Mirror (WHAM) magnetic mirror device [D. Endrizzi J. Plasma Phys. **5** (2023)]. ICRF power will be used in WHAM to accelerate high-energy neutral beam injected deuterium ions with ion cyclotron absorption at the second to fourth harmonics of deuterium. At these harmonics, for the spatial scales present in WHAM, full-wave simulations most accurately capture wave propagation, including transmission, reflection, and absorption at the cyclotron layer. The antenna is modeled as a single strap with $m = 0$ excitation, where m is the azimuthal mode number. We present some preliminary results for wave coupling and heating.

1 Introduction

The AORSA all orders spectral algorithm full wave code [1] has been applied in its 2D form to tokamaks and in its 3D form to stellarators [2]. The code uses the co-location method with a Fourier basis in all three dimensions. This permits it to represent the full wave number vector algebraically to evaluate the local Stix dielectric tensor [3] to all orders in thermal effects and retain all cyclotron harmonic wave interactions. In axisymmetric geometries a single toroidal mode is used, and separate simulations may be summed up weighted by the coupled antenna spectrum. For stellarators, toroidal modes are coupled taking advantage of the periodicity of a given stellarator geometry. AORSA also retains parallel and perpendicular equilibrium gradient effects to leading order. It is well established and has been benchmarked with other codes [4, 5]. As many new fusion concepts are being revisited by private fusion companies and public fusion research, it would be advantageous if the technical developments in AORSA could be applied to devices other than tokamaks and stellarators.

The geometry used in the modified AORSA here is cylindrical (R, θ, Z) with θ playing the role of $-\phi$ in a traditional toroidal coordinate system (r, θ, ϕ). Therefore, AORSA can in principle handle the geometry of mirrors and other cylindrical devices. The axis of revolution (the major radius R_0 in tokamaks) is 0 and the surface of revolution is the half-plane $(R \geq 0, Z)$. Figures 1 and 2 show the solution domains indicated by the gray boxes for the two types of geometries.

Past efforts often involved taking the infinite aspect-ratio limit $R_0 \to 0$ to eliminate toroidal effects. This can be done with modern RF codes developed for tokamaks with the draw back that the circular cross-section of the mirror is modeled which may be of limited interest for poloidally symmetric mirrors - meaning that only m=0 structure is in the cross-section. Some efforts at modeling the (R,Z) mirror geometry have been made in the past but only using cold collisional plasma dielectric models [6, 7].

The WHAM [8] mirror device at the University of Madison-Wisconsin and future devices being developed by the private fusion company Realta will use ion cyclotron heating (ICRF), electron cyclotron heating (ECH) and neutral beam injection (NBI) as heating sources. Since the waves used for ICRH in these devices are often comparable to the column radius in size, a full-wave approach is desirable. Since AORSA also includes arbitrary ion or electron harmonics in its model, it can also capture the higher harmonic interactions that take place in the high field regions at the ends of the devices. This is particularly relevant for devices such as WHAM which use high-field HTS magnets.

In the subsequent sections, we describe in further detail the modifications to AORSA necessary to run in mirror geometry. We then present results in two mirror scenarios, WHAM and a generic end plug scenario that show different limits of full-wave behavior in mirrors. We then conclude with a discussion of future development.

2 Modifications to AORSA

The cylindrical geometry of the AORSA code developed for tokamak and stellarator geometries is also suited for cylindrical geometries such as mirrors as shown in Figure 2. For magnetic equilibria, the code reads in Grad-Shafranov

*Corresponding author: jcwright@mit.edu

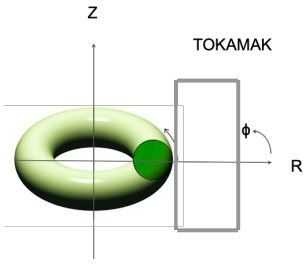

Figure 1. An example of a typical cylindrical geometric for a tokamak. The surface of revolution is centered at a major radius R_0 and R, Z coordinates are used in the solution domain.

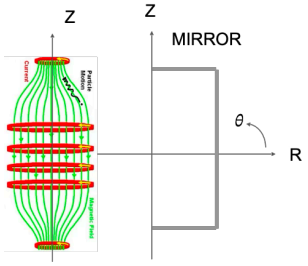

Figure 2. Cylindrical geometric applied to a mirror. The major radius is reduced to 0 and the surface of revolution is one half of the R, Z cross-section plane extending to the origin.

Table 1. Parameters for the two mirror configurations considered.

Machine	ions	T_i [keV]	R × Z [m]	f [MHz]
WHAM	D(1%H)	7	0.5 × 2.0	26.5
End Plug	T	80	0.6 × 4.5	115.5

equilibria in the `G-EQDSK` format [9]. A naive application of `AORSA` to mirror geometries would have resulted in numerous division-by-zero errors. Another assumption in the physics model was having finite values for the toroidal field and current. Because of the large aspect ratio for mirrors ($L_z/2\pi a$), we restored the `AORSA` feature of anisotropic resolution so that $NR \neq NZ$) which increases the efficiency of allocated resolution. In the plots shown in this paper, the scale in the R direction is often much smaller than in the Z direction for example.

2.1 Handling of the origin

To address the coordinate singularity at $R = 0$ it is necessary to address the use of $1/R$ through the code. This appears in calculations of field line coordinates, spatial averages, and values of poloidal field coordinates by $\nabla\psi \times \phi/R$. These points, once identified, are straight forward to address by equivalent formulations or limiting values at the axis. For the wave electric field, rather than a conducting wall condition at the left boundary a regularity or natural boundary condition should be used. This is the case for `AORSA` if no conducting boundary is imposed at $R = 0$.

2.2 Vanishing "toroidal" field

In cylindrical geometry (R, ϕ, Z), the cylindrical angle of ϕ, sometimes called θ, is the toroidal direction ϕ in (r, θ, ϕ) with a sign depending on the COCOS convention [10]. Typically, the toroidal current and safety factor will vanish, requiring care where these quantities may be used. The magnetic equilibrium toroidal field component vanishes in mirrors and often in other cylindrical geometries such as FRCs or magnetic dipoles such as LDX [11]. Flux surface averages for radial power profiles and exporting of velocity space diffusion coefficients for use in Fokker-Planck codes involve integration along field lines to establish closed flux surfaces (`AORSA` does not require closed flux geometry) or for bounce/transit averages of ions and electrons. In this case, the independent coordinate for integration is the distance along the field line rather than the toroidal angle.

3 Applications to mirrors

With the modifications in the previous section the `AORSA` code can simulate ICRH in mirror-like geometries – defined as those for which the axis of symmetry lies at $R = 0$. Table 1 gives the parameters for two mirror scenarios considered. Placing the ICRH antenna near the end of the central cell where the high field magnet is located applies the RF where the ions have their turning points. In Fig. 3, the labeled lines indicate the deuterium resonances for the WHAM scenario with $B(0) = 0.5\ T$, $B(\pm 1m) = 12\ T$. Placing the antenna at $Z = -0.62m$ positions it near the ion turning points and between the first and second cyclotron harmonics. The end plug scenario from the Appendix of [12] is similar except the harmonics are for a tritium plasma as shown by the white lines in Fig. 6 and the antenna is at $Z = -1.5m$.

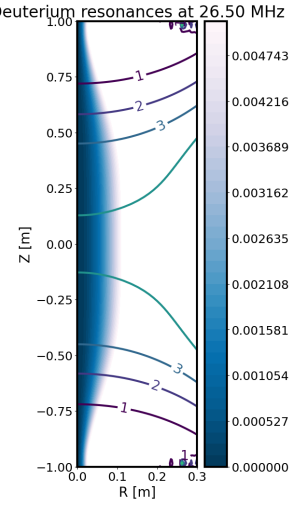

Figure 3. The location of ICRF resonances in the WHAM device. Legend indicates poloidal flux magnitude and labeled lines the deuterium resonance harmonics.

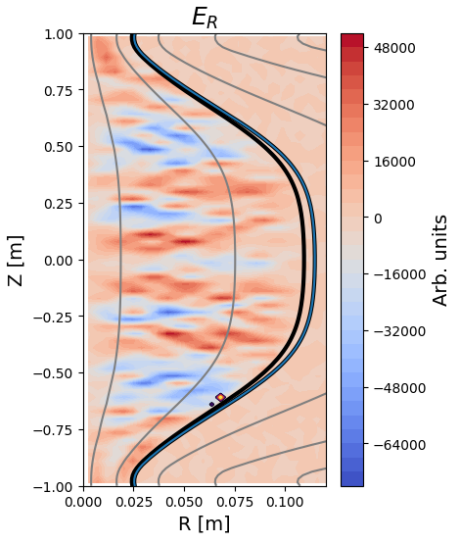

Figure 4. The orange diamond near the limiting surface indicates the antenna location. The radial electric field component has alternating positive and negative contours showing the presence of a standing wave pattern. AORSA grid is NR=32 x NZ=64.

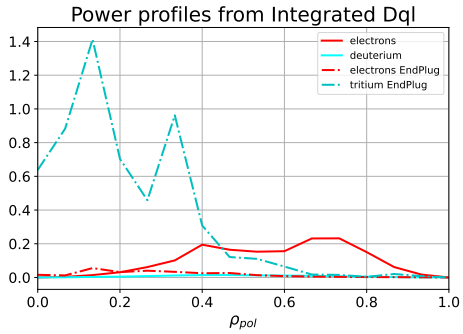

Figure 5. RF power deposition by species as calculated from the quasilinear flux acting on a maxwellian distribution. Solid lines show heating in the WHAM device and dashed lines show the End Plug configuration. Power densities are normalized to the coupled power and the volume of the devices for purposes of comparison.

The antenna used is a single continuous strap driving a broad $k_\parallel$ spectrum peaked at $k_\parallel = 0$ with no azimuthal variation ($m = 0$). There are two consequences to this: 1) the parallel wave has no large conserved component like the toroidal component in a tokamak, indeed there is no k_θ component in the plasma response regardless of the antenna design, and 2) the cavity plays a role in selecting $k_\perp$ and therefore $k_\parallel$ through the dispersion relation. This later point can result in volume filling cavity modes in small devices with weaker damping. The situation improves with larger devices, higher ion temperatures and multiple antenna straps enabling a degree of spectrum control and elimination of low $k_\parallel$ modes.

The AORSA simulation of the WHAM RF scenario with a single antenna strap produces standing wave patterns and consequently poor core deposition with power lost in the cool edge plasma and a low antenna loading resistance of 0.005 Ohms as in Fig. 4. The plasma selects the first mode from broadband antenna that fits in the plasma such that a cavity mode with perpendicular wavelength on the order of the minor radius dominates. This mode has a large component of kinetic flux and so the wave power reversibly sloshes between the field and the plasma. In practice, large edge losses and poor antenna loading would be seen. Fig. 5 presents radial power deposition profiles by species as calculated by the RF driven quasilinear flux acting on a Maxwellian distribution. This method excludes the sloshing kinetic flux and is positive definite. We see that the RF heating is on the electrons with a small amount of damping on the deuterium. This is because there are only a few axial wavelengths in this device.

The end plug design analyzed here is larger than WHAM. Its dimensions are given in meters with radius and full axial length. An 100 keV tritium neutral beam generates an 80 keV hot ion population leading to strong ion damping of ICRH. In Fig. 6 the left-hand polarized component has increased amplitude at the 2nd and 3rd tritium cyclotron harmonics indicating strong damping. The higher wave frequency creates shorter wavelength and the higher temperature from the beam heating increases the damping resulting in a more typical scenario with a propagating rather than standing wave. This case has heating partition of approximately 80% tritium and 20% electrons. The radial power deposition curves for this case are also in Fig. 5 and show a narrow core deposition as expected with stronger absorption. The antenna loading for this case was 0.05 Ohms. In absolute terms loading for both cases is low but now optimization of antenna placement has been done for this study.

4 Conclusions

The AORSA code has been modified to perform full-wave simulations in mirror geometries. This is particularly needed when wavelengths are on the order of the device radius. The all orders algorithm also captures high harmonic resonant interactions near the high-field ends of the mirror geometries. In this paper, we have shown two cases, WHAM and an end plug setup, that demonstrate two types of wave behavior. The first produces a standing wave pattern with weak damping globally on electrons. The second - larger and hotter device - shows a more strongly damped propagating mode with power deposited at ion harmonics. Future work will explore non-Maxwellian effects with a Fokker-Planck code for the mirror. We will also explore optimization of the antenna spectrum with multiple antennas and optimization of antenna placement. With these updates, AORSA will provide a tool for modeling RF waves in cylindrical devices with thermal effects.

5 Acknowledgments

Work supported by US DOE Contract No. DE-FG02-91-ER54109 and Realta Fusion.

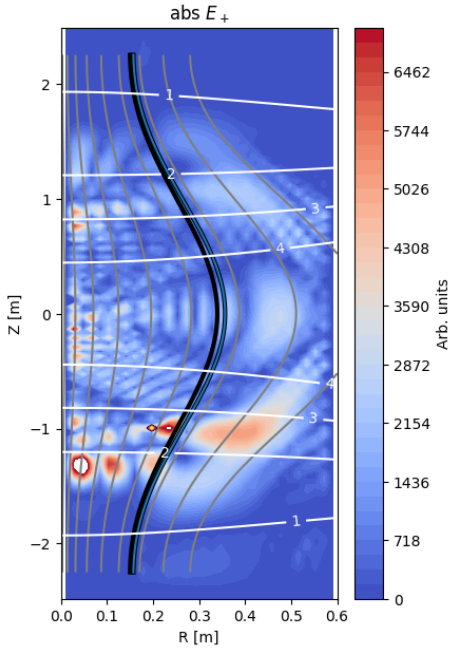

Figure 6. White contour lines indicate Tritium resonances. Antenna is at R=0.22m Z=-1m indicated by red diamond. Black contour is the limiting flux surface. Left hand polarized component is shown. The grid resolution is (NR,NZ)=(32,128).

References

[1] E.F. Jaeger, L.A. Berry, D.B. Batchelor, M.D. Carter, All-orders spectral calculation of radio-frequency heating in two-dimensional toroidal plasmas, Phys. Plasmas **8**, 1573 (2001). https://doi.org/10.1063/1.1359516

[2] E.F. Jaeger, L.A. Berry, E. D´Azevedo, D.B. Batchelor, M.D. Carter, K.F. White, Advances in full-wave modeling of radio frequency heated, multidimensional plasmas, Phys. Plasmas **9**, 1873 (2002). https://doi.org/10.1063/1.1455001

[3] T.H. Stix, Waves in Plasmas (American Institute of Physics, New York, 1992)

[4] J.C. Wright, P.T. Bonoli, M. Brambilla, F. Meo, E. D´Azevedo, D.B. Batchelor, E.F. Jaeger, L.A. Berry, C.K. Phillips, A. Pletzer, Full wave simulations of fast wave mode conversion and lower hybrid wave propagation in tokamaks, Phys. Plasmas **11**, 2473 (2004). https://doi.org/10.1063/1.1652731

[5] R.V. Budny, L. Berry, R. Bilato, P. Bonoli, M. Brambilla, R.J. Dumont, A. Fukuyama, R. Harvey, E.F. Jaeger, K. Indireshkumar et al., Benchmarking ICRF full-wave solvers for ITER, Nucl. Fusion **52**, 023023 (2012). https://doi.org/10.1088/0029-5515/52/2/023023

[6] E. Jaeger, D. Batchelor, H. Weitzner, J. Whealton, ICRF wave propagation and absorption in tokamak and mirror magnetic fields – a full-wave calculation, Computer Physics Communications **40**, 33 (1986). http://doi.org/10.1016/0010-4655(86)90147-5

[7] M. Phillips, A. Todd, The numerical solution of icrf fields in axisymmetric mirrors, Computer Physics Communications **40**, 65 (1986). https://doi.org/10.1016/0010-4655(86)90148-7

[8] D. Endrizzi, J. Anderson, M. Brown, J. Egedal, B. Geiger, R. Harvey, M. Ialovega, J. Kirch, E. Peterson, Y.e.a. Petrov, Physics basis for the wisconsin hts axisymmetric mirror (WHAM), J. Plasma Phys. **89**, 975890501 (2023). https://doi.org/10.1017/S0022377823000806

[9] L. Lao, J. Ferron, R. Groebner, W. Howl, H. St. John, E. Strait, T. Taylor, Equilibrium analysis of current profiles in tokamaks, Nuclear Fusion **30**, 1035 (1990). https://doi.org/10.1088/0029-5515/30/6/006

[10] O. Sauter, S. Medvedev, Tokamak coordinate conventions: Cocos, Computer Physics Communications **184**, 293 (2013). https://doi.org/10.1016/j.cpc.2012.09.010

[11] D.T. Garnier, A.K. Hansen, J. Kesner, M.E. Mauel, P.C. Michael, J.V. Minervini, A. Radovinsky, A. Zhukovsky, A. Boxer, J.L. Ellsworth et al., Design and initial operation of the LDX facility, Fusion engineering and design **81**, 2371 (2006). https://doi.org/10.1016/j.fusengdes.2006.07.002

[12] S.J. Frank, J. Viola, Y.V. Petrov, J.K. Anderson, D. Bindl, B. Biswas, J. Caneses, D. Endrizzi, K. Furlong, R.W. Harvey et al., Confinement performance predictions for a high field axisymmetric tandem mirror, arXiv (2025), 2411.06644. https://arxiv.org/abs/2411.06644